



Mapping signalling perturbations in myocardial fibrosis via the integrative phosphoproteomic profiling of tissue from diverse sources

Uros Kuzmanov^{1,2,10}, Erika Yan Wang^{3,10}, Rachel Vanderlaan⁴, Da Hye Kim^{1,2}, Shin-Haw Lee^{1,2}, Sina Hadipour-Lakmehsari^{1,2}, Hongbo Guo¹, Yimu Zhao³, Meghan McFadden¹, Parveen Sharma⁵, Filio Billia^{6,7}, Milica Radisic^{3,8}✉, Anthony Gramolini^{1,2,6}✉ and Andrew Emili⁹✉

Study of the molecular basis of myocardial fibrosis is hampered by limited access to tissues from human patients and by confounding variables associated with sample accessibility, collection, processing and storage. Here we report an integrative strategy based on mass spectrometry for the phosphoproteomic profiling of normal and fibrotic cardiac tissue obtained from surgical explants from patients with hypertrophic cardiomyopathy, from a transaortic-constriction mouse model of cardiac hypertrophy and fibrosis, and from a heart-on-a-chip model of cardiac fibrosis. We used the integrative approach to map the relative abundance of thousands of proteins, phosphoproteins and phosphorylation sites specific to each tissue source, to identify key signalling pathways driving fibrosis, and to screen for anti-fibrotic compounds targeting glycogen synthase kinase 3, which has a consistent role as a key mediator of fibrosis in all three types of tissue specimen. The integrative disease-modelling strategy may reveal new insights into mechanisms of cardiac disease and serve as a test bed for drug screening.

Cardiovascular diseases are a global epidemic responsible for 17.7 million deaths worldwide annually, and are predicted to remain one of the leading causes of mortality in the developed world¹. However, the molecular mechanisms driving pathological initiation and progression of these diseases are probably multifaceted and largely unknown, complicating the direction of treatment. Identification of the signalling cascades and molecular processes that are perturbed over the disease course in clinical samples and experimental models of cardiac pathology is required to improve the early detection, monitoring and management of chronic cardiovascular diseases.

Hypertrophic cardiomyopathy (HCM) is the most commonly inherited heart condition. It is typically caused by mutations in genes coding for sarcomere proteins². Myocardial fibrosis is a hallmark of HCM and is considered a major contributing factor to development of tachyarrhythmias and the development of heart failure^{3–5}. Fibrosis often occurs naturally following other cardiovascular diseases, such as ischaemic and non-ischaemic cardiomyopathies, and is characterized by cardiac fibroblast overproliferation, myofibroblast activation and increased deposition of fibrous extracellular matrix (ECM) proteins⁶. Recent studies on early-stage HCM models and patients have provided insight into the direct interplay between sarcomere mutations and fibrosis that may precede the development of cardiac hypertrophy⁷. These mechanisms include activation of pro-fibrotic pathways and increased collagen synthesis before visible structural cardiac remodelling, implicating fibrosis as a primary contributor to the pathophysiologic development of HCM^{4,8}. However, the under-

lying molecular signalling mechanisms driving fibrotic progression, which are attractive as potential targets of therapeutic intervention, remain poorly understood.

Understanding and targeting perturbed signalling cascades in patients is of crucial clinical importance. In addition to the high-throughput profiling of clinical samples in search of new diagnostic and therapeutic modalities, future screening, testing and validation of large numbers of potential therapeutics from existing chemical libraries will require a model of cardiac fibrosis that is both simple and representative, and a reproducible methodology to record and analyse molecular changes that occur as a result of pathological onset or chemical intervention.

Recent advances in tissue engineering and microfabrication technologies have contributed to the emergence of organ-on-a-chip (OOC) models for emulating human biology⁹. This technique enables the development of three-dimensional (3D) biomimetic systems with intricate structural and functional characteristics of human organs. The recently developed Biowire II, a heart-on-a-chip model for cultivating miniaturized engineered cardiac tissues, uses human induced pluripotent stem cell (hiPSC)-derived cardiomyocytes to generate cardiac tissue capable of promoting structural and functional maturation^{10,11}. Biowire II can capture pathological contractile phenotypes using tissue derived from patients with left ventricular hypertrophy or biomimetic disease conditions¹². The Biowire model has also shown increased utility in high-content screening of large numbers of potential therapeutics by screening a library of kinase inhibitors for their effects on cardiac function¹³,

¹Ted Rogers Centre for Heart Research, University of Toronto, Toronto, Ontario, Canada. ²Department of Physiology, University of Toronto, Toronto, Ontario, Canada. ³Institute of Biomaterials and Biomedical Engineering, University of Toronto, Toronto, Ontario, Canada. ⁴Division of Cardiac Surgery, University of Toronto, Toronto, Ontario, Canada. ⁵Institute of Translational Medicine, University of Liverpool, Liverpool, UK. ⁶Toronto General Research Institute, Toronto, Ontario, Canada. ⁷Division of Cardiology, University Health Network, Toronto, Ontario, Canada. ⁸Department of Chemical Engineering and Applied Chemistry, University of Toronto, Toronto, Ontario, Canada. ⁹Departments of Biochemistry and Biology and the Centre for Network Systems Biology, Boston University School of Medicine, Boston, MA, USA. ¹⁰These authors contributed equally: Uros Kuzmanov, Erika Yan Wang.
✉e-mail: m.radisic@utoronto.ca; anthony.gramolini@utoronto.ca; aemili@bu.edu

compared with the commonly used 2D-monolayer cardiomyocyte culture. We also recently demonstrated that fibrotic Biowires capture key functional hallmarks of fibrosis, including increased myofibroblast presence, collagen deposition and stiffness in fibrotic Biowires compared with controls¹⁴.

Identifying global signalling-pathway perturbations at the phenotypic level in patient samples and disease models requires the use of precision mass spectrometry-based proteomic and systems biology approaches. Implicit to the entire OOC field is a hypothesis that OOC devices with human cells are more similar at the protein level to native human tissues compared with commonly available rodent models and that these similarities will enable facile and correct identification of small-molecule effects on human tissues. In this study, we set out to test this hypothesis for the Biowire heart-on-a-chip model.

Additionally, phosphoproteomic approaches provide even more complete coverage by enabling monitoring of protein phosphorylation involved in quick and reversible control of molecular signalling, as we have previously demonstrated¹⁵. Relatively few studies to date have examined phosphorylation dynamics in heart tissue explants, including a single analysis of a pressure-overload mouse model¹⁶, examination of β -adrenergic signalling in mouse cardiac tissue¹⁷, and several profiling clinical samples^{18–20}. Although several prominent proteomic profiling studies have been conducted on cardiomyocytes derived from induced pluripotent stem cells^{21,22}, to our knowledge, there are no global phosphoproteomic studies examining OOC models of cardiac disease, obscuring their correspondence to human disease.

We report the development and application of an unbiased quantitative mass spectrometry-based workflow, which is standardized from sample preparation to data analysis and designed for parallel monitoring of signalling pathways in quantity-limited OOC cardiac fibrosis models, clinical samples and animal tissue. Using deep global phosphoproteomic profiling as a unified and mechanistically informative framework, we analysed and characterized the signalling perturbations in the Biowire model of fibrotic cardiac tissue compared with cardiac specimens from patients with HCM and an established transverse aortic constriction (TAC) mouse model of cardiac hypertrophy and fibrosis. All disease-affected sample types were compared with matched non-pathological control tissues. This systematic analysis resulted in the identification and relative quantification of thousands of proteins, phosphoproteins and phosphorylation sites across the complete sample cohort. Furthermore, for each set of analysed experiments, the generation of deep quantitative data enabled statistical pathway-enrichment analysis, revealing selective disruptions in dozens of specific biological processes and signalling pathways, providing potentially clinically actionable information on the progression and maintenance of fibrotic mechanisms in cardiac pathology.

Among the panel of affected kinases in cardiac fibrosis remodeling indicated by phosphoproteomic analysis of the different sample types, altered protein levels and differential expression of phosphorylation sites within consensus motifs targeted by glycogen synthase kinase 3 (GSK3) indicated a role of this kinase as a key mediator of fibrosis. To confirm the physiological relevance of the analysis and validate the efficacy of our model system in screening new anti-fibrotic compounds, we evaluated four unprofiled GSK3 inhibitors from a well-characterized small-molecule kinase-inhibitor library²³. The Biowire II model enabled non-invasive screening of potential anti-fibrotic compounds based primarily on their ability to inhibit collagen deposition and attenuate passive tension.

In addition to enabling precise molecular analysis of clinical, in vitro and animal model samples, the combined (OOC, animal model and clinical specimen) analytical framework for exploring human disease mechanisms provides a unified high-content approach for identifying functionally relevant clinical targets and for screening bioactive compounds, drug leads and potential thera-

peutics for cardiovascular diseases and other pathologies relying on simple-to-implement OOC models.

Results

Comparative phosphoproteome analysis. To achieve a global survey of signalling cascades affected by cardiac pathology and the onset of fibrosis, we developed a three-tiered methodology for comparative quantitative proteomic and phosphoproteomic profiling on three sets of relevant samples and respective controls: (1) cardiac Biowire constructs generated using cardiomyocytes derived from hiPSCs, representing a fibrotic phenotype and normal controls; (2) cardiac tissue acquired from patients with HCM who are undergoing septal myectomy and patients with left ventricular outflow tract (LVOT) obstruction who underwent myectomy surgery (unfolded aorta is used as non-HCM control); and (3) heart tissue from 12-week-old mice that have undergone TAC for 4 weeks (resulting in cardiac hypertrophy) and control sham-treated mice (Fig. 1). Due to the low protein amounts associated with small OOC tissues and the heterogeneity associated with tissue explants requiring increased reliability of quantification, we subjected the clinical samples, TAC mouse heart tissue and cardiac Biowire constructs to a phosphoproteomic multiplexing strategy based on isobaric chemical-tag labelling (TMT) (see Methods). To increase coverage, samples were also prefractionated using HILIC to resolve the mixtures of negatively charged phosphopeptides²⁴. Finally, due to the low relative abundance of phosphopeptides and mass spectrometry signal suppression arising from the increased negative charge resulting from the phosphate moiety, an additional round of affinity enrichment of phosphopeptides was performed using immobilized TiO_2 affinity chromatography. A schematic of the experimental workflow is presented in Fig. 1.

Fibrosis in analysed samples. Engineered Biowire control and fibrotic tissues were constructed using hiPSC-derived cardiomyocytes and human cardiac fibroblasts in a hydrogel designed on the basis of mechanical property tests^{25,26}. Over the course of culturing, fibroblasts remodel the tissue structure differently in the normal and fibrotic tissues, as indicated by tissue compaction and polymer-wire bending (Supplementary Fig. 1). The gel compaction in fibrotic tissues is significantly faster than in the controls, and the deflection of polymer wires caused by the cell-tractional forces as measured by passive tension is consistently larger in the fibrotic Biowires compared with the controls (Supplementary Fig. 1). This is accompanied by a markedly lower active contractile force in the fibrotic group compared with the control group (Supplementary Fig. 1). Passive tension in the fibrotic tissues continues to increase with time in culture after the tissue dimension has stabilized, indicating ongoing fibrotic remodelling (Supplementary Fig. 1).

Second-harmonic generation (SHG) is a label-free quantitative imaging technique used to visualize collagen content at tissue level. An increase of fibrillar collagen accumulation was visualized by SHG under a laser-scanning microscope in the fibrotic Biowire tissues compared with the control group (Fig. 2a). Similarly, collagen-rich areas were more abundant in cardiac sections from patient and four-week post-TAC mouse compared with control groups (Fig. 2b,c). The fibrotic tissues deposited increased ECM glycoproteins indicative of fibrotic plaque development, as determined by immunofluorescence staining with wheat germ agglutinin (WGA) (Supplementary Fig. 2). Similarly, immunofluorescence imaging of patient and four-week post-TAC mouse cardiac sections stained for WGA and α -actinin revealed more infiltrating fibrosis in the cardiac myocytes in pathological hypertrophy (Supplementary Fig. 2) and a more disorganized sarcomeric pattern.

Overview of proteomic and phosphoproteomic coverage in analysed samples. We identified 6,587 proteins and phosphoryla-

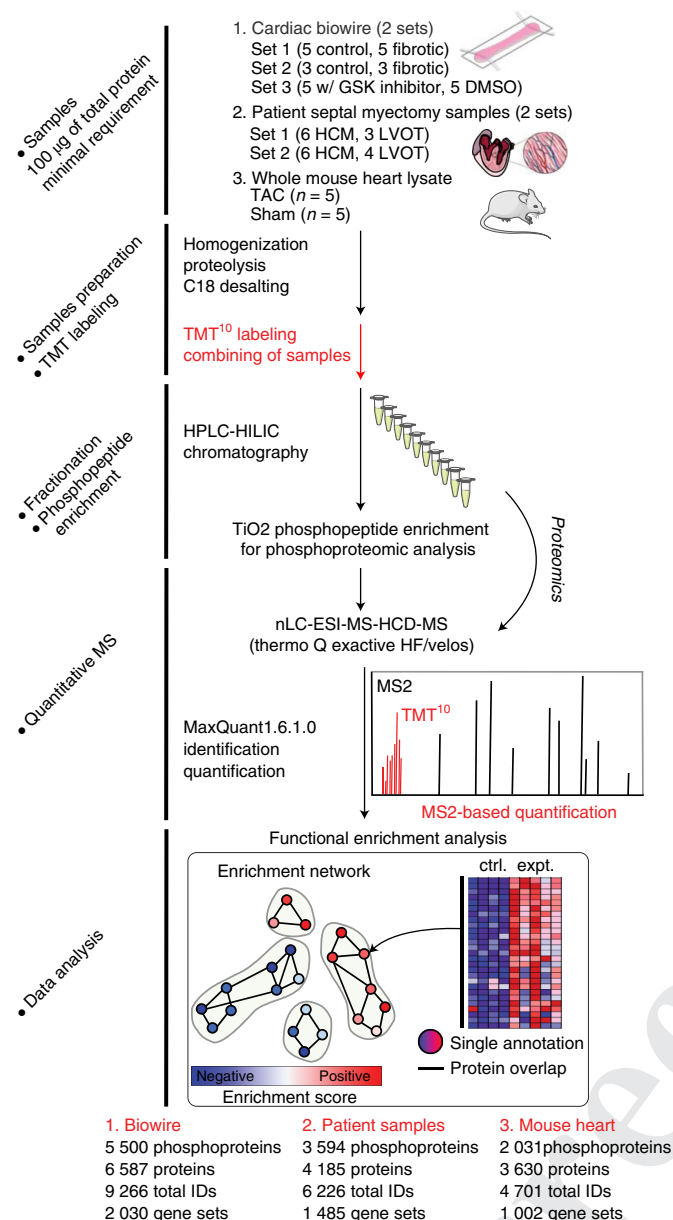


Fig. 1 | Overview of phosphoproteomic workflows. Septal-myectomy tissue explants (from patients with hypertrophic cardiomyopathy (HCM) and patients with unfolded aortas), cardiac Biowires (control, fibrotic and fibrotic treated with GSK3 inhibitor), mouse hearts (four-week transverse aortic constriction (TAC) and sham-treated mice) were analysed with a workflow based on liquid chromatography with tandem mass spectrometry. Ctrl, control; Expt, experimental sample; DMSO, dimethylsulfoxide; HILIC-HPLC, hydrophilic-interaction liquid chromatography-high performance liquid chromatography; LVOT, left ventricular outflow tract.

ditions in the different datasets (Fig. 3b, Supplementary Fig. 3 and Supplementary Data 1 and 2). The higher throughput and lower variability in the multiplexed measurements demonstrate the utility of our approach when dealing with samples limited by protein amount (that is, OOC and patient explants) as indicated by the high degree of quantitative value distribution and correlation across all sample types (Supplementary Fig. 4).

Global data comparison. In direct comparisons of the different datasets, the Biowire OOC model system exhibited more consistent and distinct changes when comparing samples with respect to both global protein expression and phosphorylation levels (Figs. 3b and 4). In the three samples from the cohort of patients with HCM carrying a heterozygous truncating mutation in *MYBPC3*, we observed a consistent decrease at both the protein and phosphorylation-site level for *MYBPC3* compared with unfolded aorta LVOT control and patients with HCM without the *MYBPC3* mutation in patient dataset 1 (Fig. 3c and Supplementary Table 1).

Additionally, a large overlap at both identified protein and phosphoprotein and functional annotation levels was observed between the Biowire phosphoproteome and proteome and another recent proteomic dataset in the context of induced pluripotent stem cell-derived ventricular cardiomyocytes (Supplementary Fig. 5), with the presented Biowire datasets providing deeper coverage and more reliably quantifiable phosphoprotein and proteins due to our TMT-labelling strategy²².

Supervised and unsupervised statistical analyses of the merged proteomic and phosphoproteomic datasets obtained for the Biowire model system were visualized using hierarchical clustering (Fig. 4a and Supplementary Fig. 3) and principal component analysis (Fig. 4b), respectively. The control specimens clearly segregated from samples reflecting pathological conditions, and the segregation was most distinct in the Biowire OOC group, which is important for downstream drug discovery studies. In the case of the patient samples and mouse heart tissue, while there is no clear discrimination based on hierarchical clustering, class separation was observed with principal component analysis, albeit with a smaller proportion of components. For the clinical data, the reference samples were generally more similar to each other, while there was higher variability among the HCM specimens, in line with the observed heterogeneity associated with the phenotypic manifestation of HCM.

Pathway-level comparison. A statistical overrepresentation test was applied to systematically evaluate the biological annotations corresponding to the totality of acquired data (that is all identified proteins and phosphoproteins) across all sample types or datasets²⁷. Notably, substantial overlap was observed among overrepresented annotations associated with Reactome pathways²⁸ and Gene Ontology (GO)^{29,30} for biological process, subcellular distribution and protein function terms (Fig. 5a and Supplementary Data 3). Commonly identified enrichments revealed structural, signalling, ion-binding, ion-channelling and metabolic proteins in disparate subcellular locations, ranging from the plasma membrane to individual organelles, many with established links to heart muscle and cardiac tissue function. Protein and phosphoprotein coverage in Biowire cardiac constructs revealed high combined annotation overlap with the other two tissue datasets (that is, 73.7% for Reactome pathways, 83.8% for GO biological process, 86.6% for GO cellular component and 88.6% for GO molecular function).

In order to use quantitative information in functional enrichment analyses, the proteomic and phosphoproteomic protein-level data were merged and rank-weighted on the basis of the significance of the change between experimental conditions in all datasets (Fig. 5b). Enrichment analysis³¹ was then used in conjunction with a custom annotation database containing information from a compendium of publicly available databases (that is, GO, Kyoto

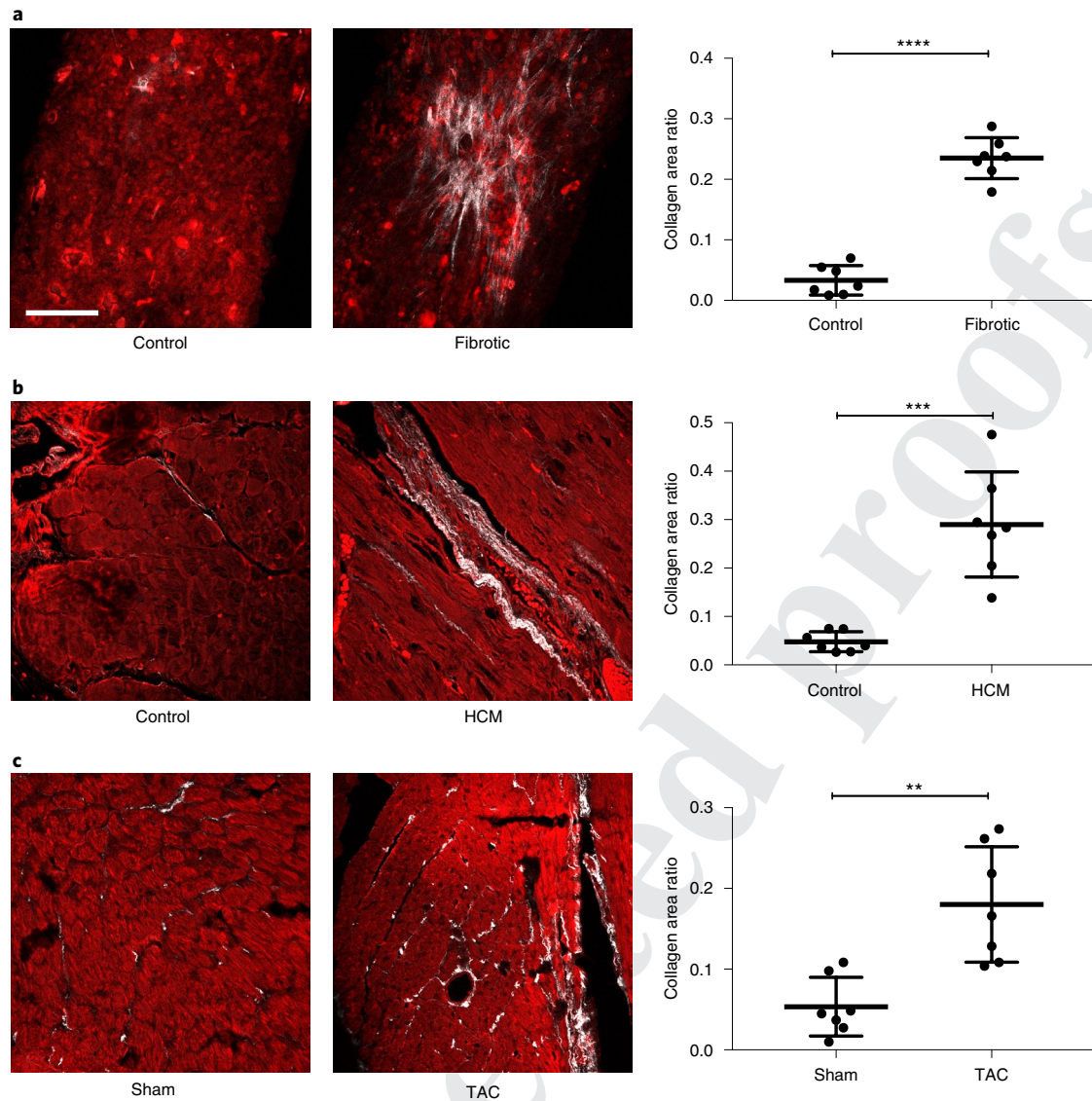


Fig. 2 | Collagen deposition in normal and fibrotic samples. a–c. Representative SHG images of fibrotic and control samples (red, tissue autofluorescence; white, collagen; scale bar, 100 μ m) and corresponding quantification. Twenty-one images were taken from seven biological replicates per group. Statistical significance was calculated using a two-tailed Student's *t*-test. **a**, Representative SHG images of normal and fibrotic Biowires and corresponding quantification of collagen area ratio (mean \pm s.d., $n=7$). **** $P < 0.0001$. **b**, Representative SHG images of cardiac sections from patients with HCM that were unaffected (control) and affected by fibrosis (HCM), and corresponding quantification of collagen area ratio (mean \pm s.d., $n=7$). *** $P < 0.001$. **c**, Representative SHG images of mouse cardiac sections from sham-treated and four-week post-TAC mice, and corresponding quantification of collagen area ratio (mean \pm s.d., $n=7$). ** $P < 0.01$ ($P=0.0013$).

Encyclopedia of Genes and Genomes, MSigDB, National Cancer Institute–Nature Pathway Information Database, NetPath, Panther and Reactome). This analysis revealed very good consistency with 2,030, 1,485 and 1,002 differentially enriched gene sets for the Biowire constructs, explants and mouse cardiac tissue surveys, respectively (Supplementary Fig. 6 and Supplementary Data 4), although the overlap between all three datasets was lower (Fig. 5c).

Taking into account the design of the Biowire disease model as a fibrotic system, among the 444 gene set annotations commonly altered in all three datasets between disease and control conditions, several were directly related to fibrotic mechanisms and showed a clear trend of increased expression of individual components in the fibrotic samples (Supplementary Fig. 7). Importantly, an additional 662 gene set annotations were uniquely similar between patient and Biowire samples, compared with 154 between mouse and human

patient samples, further supporting a higher level of similarity between patient samples and Biowire, versus mouse samples. The 444 networks common to all models included gene sets associated with the matrisome, an expanded set of proteins involved in ECM deposition, organization and processing constructed from experimental observations and bioinformatic prediction of ECM proteins on the basis of protein-domain composition³². Further gene sets uniformly identified as altered across all the sample types include those with general terms involving cardiac muscle cell organization and development, cell junctions, calcium-related pathways, calmodulin binding and mitochondrial function (Supplementary Data 4).

Additional enriched signalling pathways of potential relevance to cardiac pathology were identified in human samples, although not uniformly (Supplementary Data 4). These included Fc γ receptor signalling, with a proposed role in autoimmune initiation of

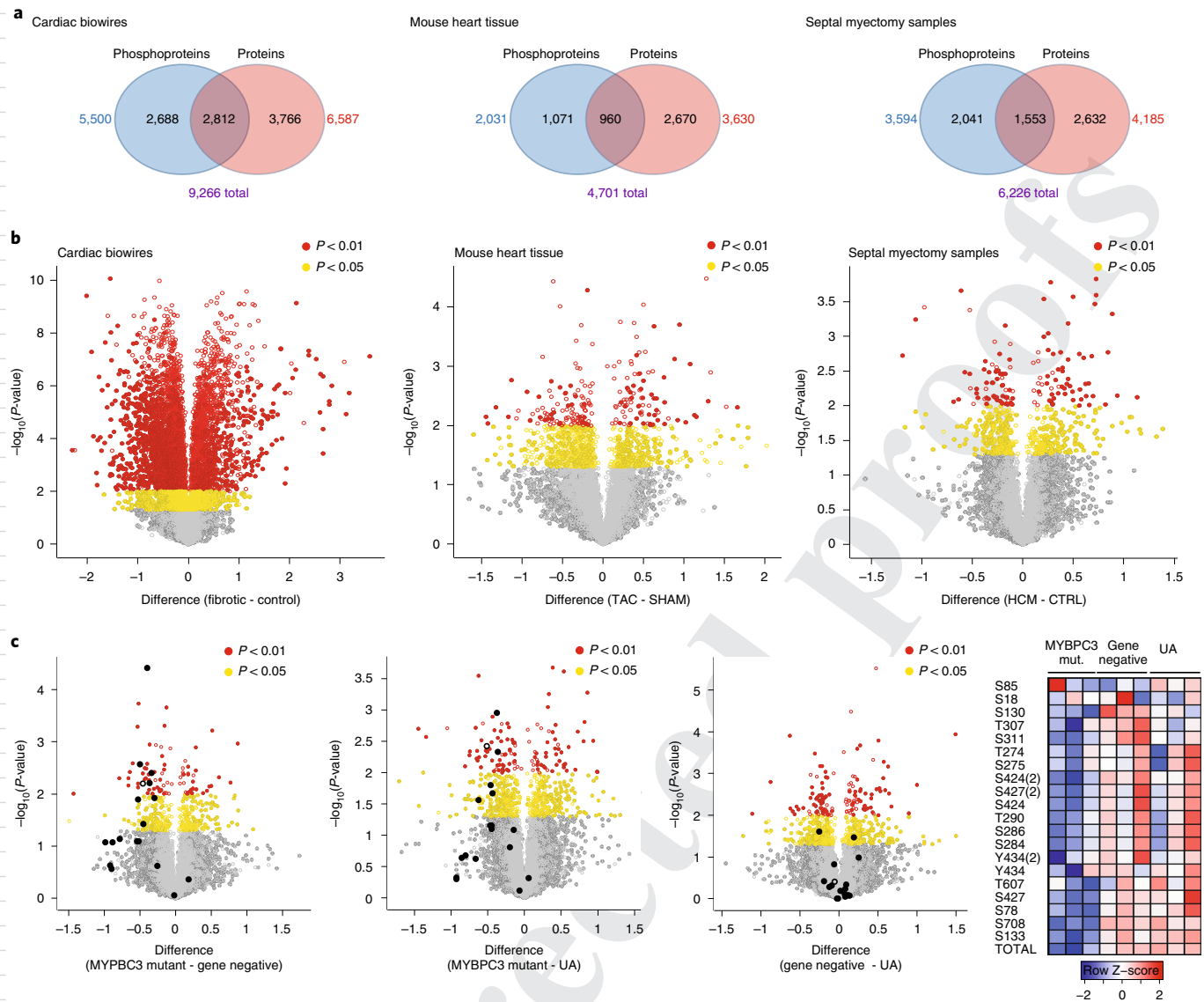


Fig. 3 | Coverage and data distribution across datasets. **a**, Venn diagram depicting the total number of proteins identified in the corresponding proteomic and phosphoproteomic datasets. **b**, Volcano plots indicating significantly altered proteins and phosphorylation sites identified in the combined proteomic and phosphoproteomic datasets from Biowires, mouse heart tissue and patient explants. Negative log-transformed P -values (two-tailed Student's t -test) associated with individual proteins (circle) and phosphorylation sites (filled circle) plotted against the difference in means of \log_2 -transformed normalized values for individual proteins and phosphorylation sites. **c**, Volcano plots indicating significantly altered proteins and phosphorylation sites identified in the merged proteomic and phosphoproteomic datasets from subgroups of septal-myectomy explants (patients with HCM with a truncating *MYBPC3* mutation, patients with HCM who are negative for the mutation, and patients with unfolded aortas (UA)). Negative log-transformed P -values (two-tailed t -test) associated with individual proteins (circle) and phosphorylation sites (filled circle) plotted against the difference in means. *MYBPC3* is highlighted in black. Heat map representing the expression of *MYBPC3* protein and phosphorylation sites across patient samples.

coronary heart disease³³, the class III histone deacetylase, with a protective role in cardiac injury³⁴, $\beta 1$ - and $\beta 3$ -integrin signalling, with established roles in cardiac fibrosis³⁵, focal adhesion kinase (FAK) signalling, involved in early-stage cardiac hypertrophy³⁶, and chemokine receptor CXCR4 signalling, with proposed roles in targeting and proliferation of progenitor cells in cardiac pathologies³⁷. These latter observations point to limitations of model systems in relation to profiling human disease.

Although occasionally identified across the different datasets, disparate signalling pathways associated with the initiation and progression of cardiac fibrosis were identified as significantly disturbed between the control conditions and mouse and Biowire experimental conditions (Supplementary Data 4), suggesting

plausible therapeutic targets. The cumulative data provided quantitative information of individual protein and phosphorylation-site components of pathways associated with the interplay of signalling networks previously linked to fibrosis, including the interrelated TGF β , WNT, β -catenin, SMAD2/3, Hedgehog, integrin-linked kinase, FAK, MAPK and PI3K–AKT–mTOR signalling cascades³⁸.

Kinase target identification. Common motifs present among the three sample groups identified kinases central to cardiac contractility, metabolism and signalling cascades (Supplementary Data 5), including consensus sequences targeted by PKA, Ca²⁺/calmodulin-dependent protein kinase II (CAMKII), ERK1/2, PKC, casein kinase 2 (CK2), CDK5 and GSK3^{39–41}.

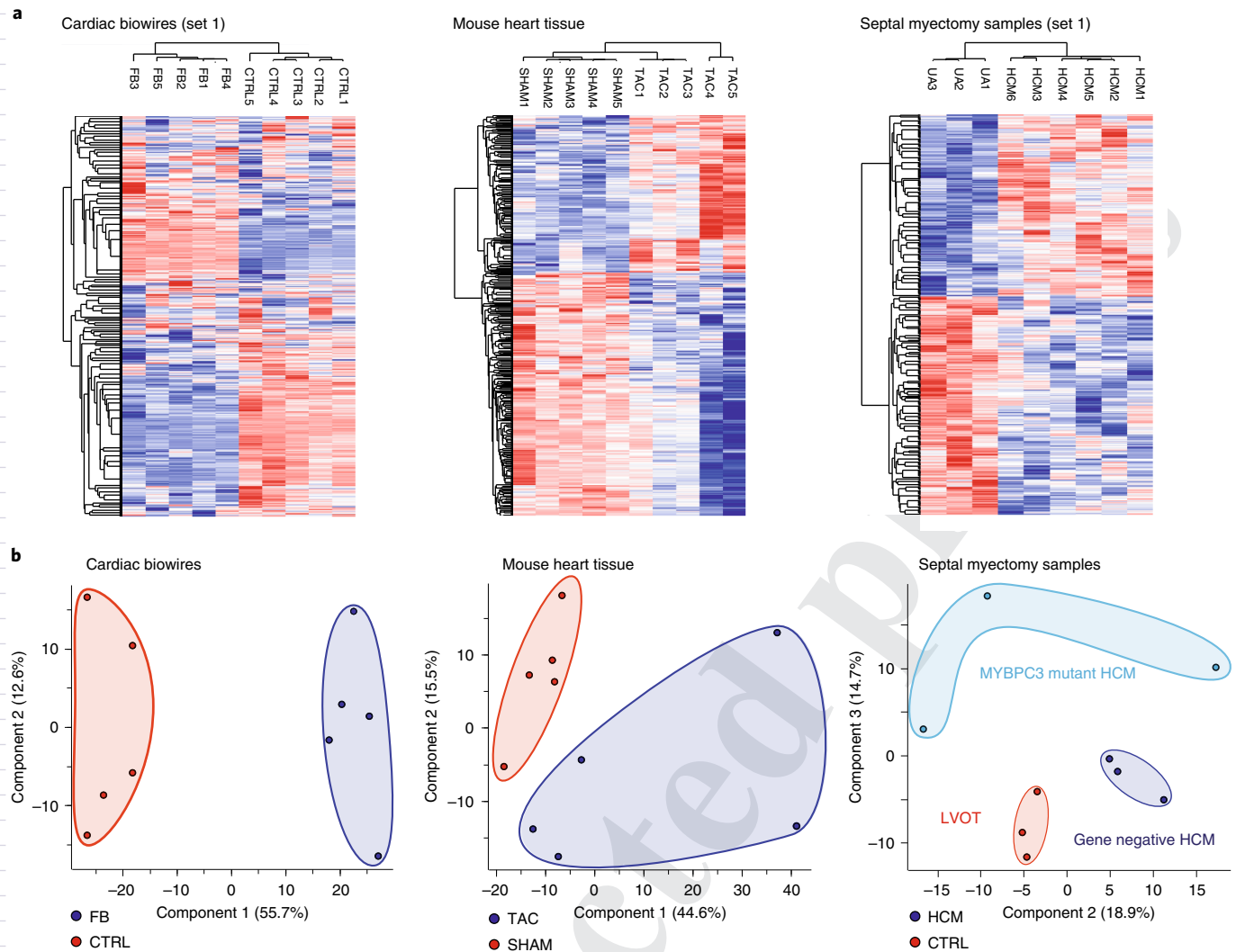


Fig. 4 | Comparison of merged proteomic and phosphoproteomic datasets between experimental and clinical conditions. a, Euclidian-distance-based hierarchical clustering of significantly altered ($P < 0.05$) proteins and phosphorylation sites in representative datasets. FB, fibroblasts. **b**, Principal component analysis of all merged proteomic and phosphoproteomic data in individual datasets.

GSK3-inhibitor screening. GSK3-substrate consensus motifs in sequences surrounding phosphorylation sites showed significant differential expression, implicating GSK3 as a mediator of fibrotic remodelling (Fig. 6, Supplementary Fig. 8 and Supplementary Data 5). To test the efficacy of the Biowire model system for screening multiple non-profiled compounds from a kinase-inhibitor set against a putative target, we evaluated four GSK3 inhibitors (GW806290X, GW827102X, GW827099X and GW828529X) from a small-molecule kinase-inhibitor library²³, together with a standard commercially available inhibitor (CHIR 99021) of GSK3. The aim was to obtain an initial proof-of-concept selection of drugs that effectively alter fibrotic remodelling and to provide important exploratory data for later trials that use different dosages and time points.

Considering the time-dependent nature of collagen deposition and fibrotic modelling, two time courses for GSK3-inhibitor treatment were investigated, specifically (1) late application of the inhibitors to already-established fibrotic tissue and (2) early application of the inhibitors at the time of tissue formation to mimic a fibrosis prevention scenario.

In (1), to assess drug effects on established fibrosis, fibrotic tissues were cultivated for six weeks under electrical conditioning

before treatment as described previously¹⁴ (Fig. 6a). We then performed a selection from the non-profiled inhibitors by evaluating compound efficacy in reducing collagen deposition and myofibroblast activation (Supplementary Fig. 9). The GW806290X-treated group showed the most significant reduction in deposited collagen in the model of already-established fibrosis, whereas the other three compounds exhibited modest or no effects on collagen inhibition, which may be related to either off-target effects or reflect the difficulty of reducing already-established fibrosis (Supplementary Fig. 9a,b). Passive tension was also used as a direct readout of fibrotic ECM remodelling in Biowires, as it is observed to be consistently higher in the fibrotic Biowires¹⁴ (Supplementary Figs. 1 and 8a). Compound GW806290X displayed the most potent effect in reducing passive tension among all GSK3 inhibitors after 7 d of treatment after maturation (Supplementary Fig. 8b), while having no negative effects on active tension (Supplementary Fig. 8c).

The anti-fibrotic efficacy of GW806290X was further validated and compared with a parallel treatment with the standard GSK3 inhibitor CHIR 99021. Similar trends in diminishing collagen deposition were observed in both treatment groups (Fig. 6b,c). By contrast, there was no statistically significant difference in myofibroblast activation between the control and GW806290X and CHIR

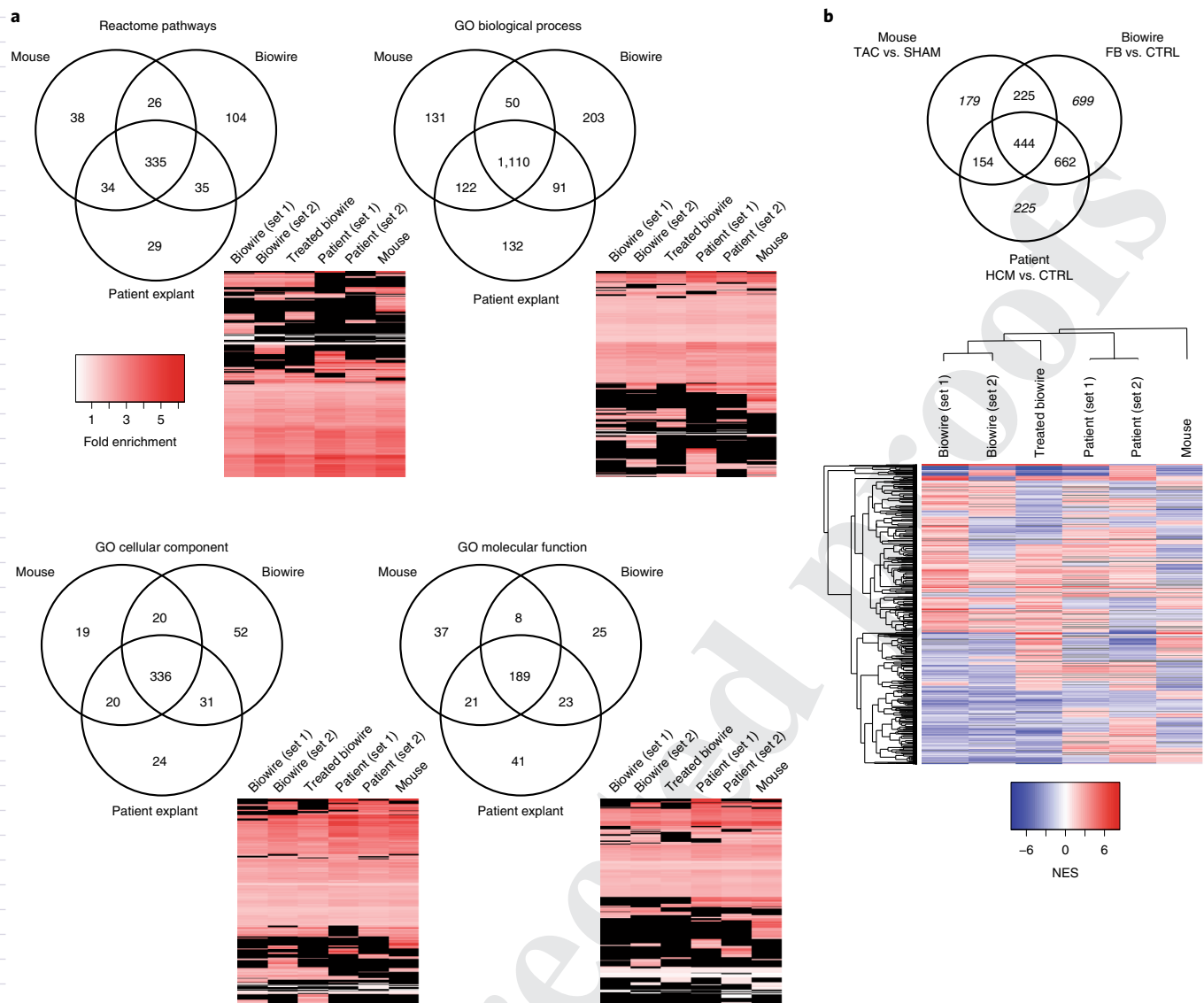


Fig. 5 | Pathway-level comparison between datasets. a, Identification-coverage comparison of significantly enriched ($P < 0.05$) annotations between datasets. Heat maps represent fold enrichment of protein or phosphoprotein IDs in the datasets over normal occurrence in the proteome. **b**, Venn diagram of overlap between GSEA significantly enriched gene sets ($P < 0.05$) and Euclidian-distance hierarchical clustergram heat map representing normalized enrichment scores of all identified gene sets.

99021 groups (Fig. 6d,e), indicating a limited ability to profoundly reduce already-established fibrosis and scarring over the time course of drug treatment that was investigated here (one week).

In (2), to investigate more effective treatment timelines and early intervention in fibrosis, treatment was also performed upon cell seeding (Fig. 7a). Significant inhibition of collagen deposition and a marked suppression of myofibroblast activation were observed after 7 d of treatment with both compounds (Fig. 7b–e), as expected. Fibroblast-guided tissue compaction reflects early fibrosis formation, with fibrotic Biowires showing faster and denser compaction^{12,14} (Supplementary Figs. 1 and 8a). Slowing of tissue compaction was observed after early treatment with GW806290X and CHIR 99021 on seeding (Supplementary Fig. 8d), accompanied by significantly lower passive tension developed at 7 d in culture (Supplementary Fig. 8e), albeit with a diminishing active force as a side effect of reduced gel compaction (Supplementary Fig. 8f).

Phosphoproteomic analysis of fibrotic Biowires treated with GW806290X (Supplementary Figs. 3 and 4) revealed a marked

decrease of significantly altered GSK3-targeted phosphorylation sites (Supplementary Fig. 10a and Supplementary Data 5) and decreased collagen expression as a result of treatment compared with controls (DMSO-treated cells; Supplementary Fig. 10b). Consistent with this, unsupervised hierarchical clustering and Gene Set Enrichment Analysis (GSEA) revealed a reversal of pathway-level phenotypes mimicking the differences seen between control and fibrotic Biowires from datasets 1 and 2 (Fig. 5c and Supplementary Figs. 6 and 7). While the number of altered targets of GSK3 (Supplementary Fig. 3 and Supplementary Data 1 and 2) between the GW806290X-treated and untreated fibrotic Biowires was lower than other comparisons (that is, fibrotic versus control Biowires, patient explants and TAC versus sham treatment), consistent with the well-established concept that multiple kinases phosphorylate the same sites and the complex interplay of compensatory mechanisms when a single kinase is specifically blocked, GSK3-targeted sites on several proteins with known roles in GSK3 signalling and/or cardiac function were significantly downregulated as the result

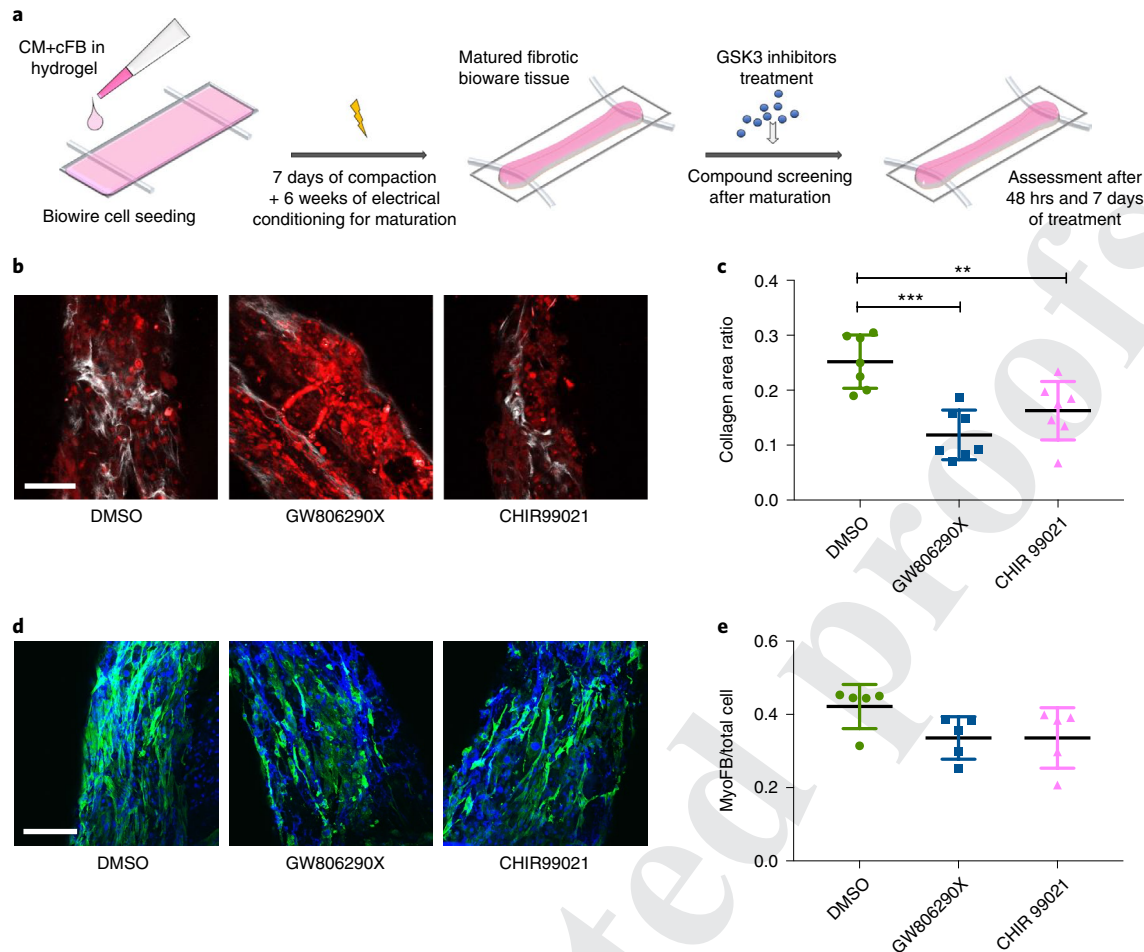


Fig. 6 | Drug treatment with the selected GSK3 inhibitor GW806290X in parallel with a standard GSK3 inhibitor (CHIR 99021) after tissue maturation.

a, Drug-screening timeline with mature Biowire tissues. **b**, Representative SHG images of fibrotic tissues treated with GW806290 and CHIR 99021 compared with DMSO control after 7 d of treatment (red, tissue autofluorescence; white, collagen; scale bar=100 μ m). **c**, Corresponding quantification of collagen area ratio from **b** (mean \pm s.d., $n > 5$). $**P < 0.01$ ($P = 0.0066$), $***P < 0.001$. **d**, Representative immunostaining of fibrotic tissues treated with GW806290 and CHIR 99021, compared with DMSO control stained for myofibroblast marker α -smooth muscle actin (α -SMA) (green), counterstained with the nuclear stain DAPI (blue) (scale bar, 100 μ m). **e**, Corresponding quantification of activated myofibroblast fraction in total cell population from **d** (mean \pm s.d., $n \geq 5$). At least 15 images were taken from at least 5 biological replicates per group for all experiments. Statistical significance was calculated using two-tailed Student's *t*-tests.

of treatment (Supplementary Fig. 10c). These included: RB1CC1, with a reported role in cardiac development⁴², YWHAB, a member of the 14-3-3 protein family involved in multiple MAPK-signalling pathways, NRSF/REST, a transcriptional repressor with an established role in the cardiac fetal gene-expression regulation⁴³, TCF12/HEB, involved in heart development and stem cell differentiation⁴⁴, ZMYND8/PRKCBP1, previously shown to regulate HIF-1 response to hypoxia in the heart⁴⁵.

Together, these results indicate the role of GSK3 as an actionable target and establish the utility of the Biowire OOC model system in screening and selecting suitable drug candidates.

Discussion

The identification and quantitative monitoring of global protein abundance and phosphorylation changes specific to a pathological state requires the application of modern phosphoproteomic techniques. Human myocardial tissue was recently analysed on a large scale by mass spectrometry-based global phosphoproteomics, which enabled the differentiation of the molecular patterns in patients with ischaemic and non-ischaemic cardiomyopathy²⁰. Systematic large-scale proteomic studies in mice have also been conducted to

determine the changes in protein phosphorylation resulting from β -adrenergic inhibition or stimulation¹⁷, and in a model of cardiac hypertrophy to determine changes due to pressure overload¹⁶, informing on the networks affected by these pathophysiological perturbations. A complementary targeted quantitative MS-based approach based on multiple-reaction monitoring has also been used to selectively measure mitochondrial-phosphoprotein involvement in cardiac physiology in mouse and human tissue samples⁴⁶. However, these studies have all been limited in either quantitative reliability, coverage or relevance to human clinical presentations. Indeed, while tandem mass spectrometry has been widely deployed for over a decade, there have been relatively few unbiased phosphoproteomic studies performed in the context of studying cardiovascular disease mechanisms, presumably due to obstacles in acquiring and processing patient samples and the generation of OOC models associated with cardiac tissue. Hence, the present study represents an experimental and data-analysis approach for documenting consistent changes in protein, phosphoprotein and pathway dynamics across patient-, mouse- and OOC-derived cardiac tissue.

TMT labelling of peptides and phosphopeptides following tryptic digestion minimizes technical errors and variability in the suc-

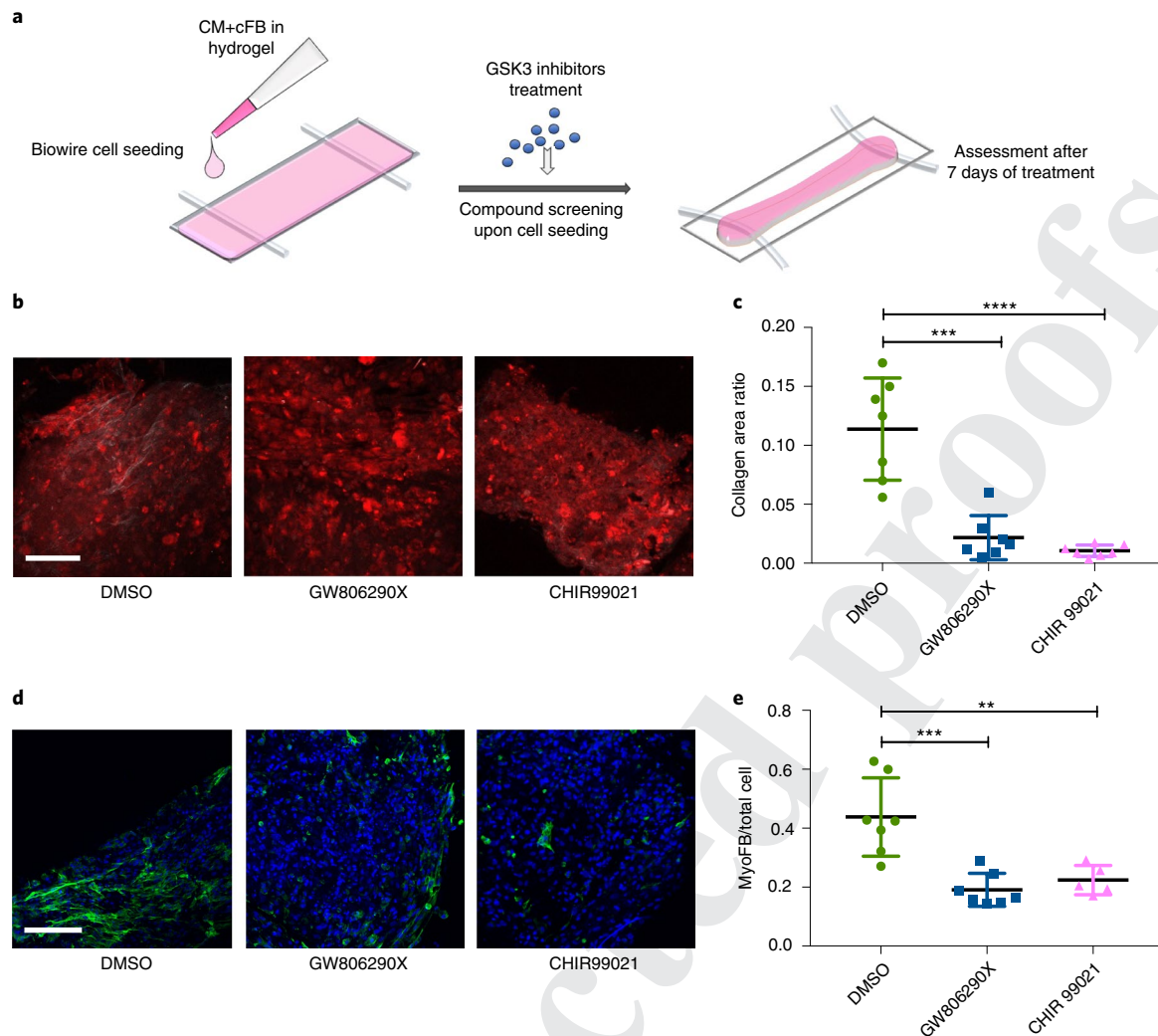


Fig. 7 | Drug screening with early treatment upon tissue seeding. **a**, Drug-screening timeline of early treatment. **b**, Representative SHG images of fibrotic tissues treated with the selected GSK3 inhibitor GW806290X in parallel with CHIR 99021 for 7 d upon seeding compared with DMSO control (red, tissue autofluorescence; white, collagen; scale bar, 100 μ m). **c**, Corresponding quantification of collagen area ratio from **b** (mean \pm s.d., $n > 5$). *** $P < 0.001$. **** $P < 0.0001$. **d**, Representative immunostaining of tissues treated with GW806290X and CHIR 99021 for 7 d upon seeding, compared with DMSO control stained for the myofibroblast marker α -SMA (green), counterstained with the nuclear stain DAPI (blue). (scale bar, 100 μ m). **e**, Corresponding quantification of activated myofibroblast fraction in total cell population from **d** (mean \pm s.d., $n \geq 5$). *** $P < 0.001$, ** $P < 0.01$ ($P = 0.0068$). At least 15 images were taken from at least 5 biological replicates per group for all experiments. Statistical significance was calculated using two-tailed Student's *t*-tests.

cessive sample preparation steps, which affects the reliability of quantitative data, due to the mixing and subsequent equal experimental handling and mass spectrometric detection of all labelled samples. This is especially true for phosphoproteomic workflows targeted to MS analyses of cardiac muscle tissue, where to ensure deeper coverage and protein or phosphoprotein detection, multiple chromatographic-fractionation and affinity-enrichment experimental steps are required, each with its own set of associated technical errors. A major limiting factor of this approach, in this and other similar TMT- or isobaric-labelling studies, is the limited number of samples that can be analysed. However, the alternative to achieving comparable coverage, requiring the same general experimental procedure and larger sample amounts in label-free experimental workflows would require (compared with a TMT-10plex experiment) about ten times as much: protein sample from each patient or model system, time/labour required for chromatographic-fractionation steps, phosphopeptide-enrichment steps and mass spectrometry time; and all at the expense of quantitative reliability of the data due

to the technical error introduced by separate processing of individual samples. The alternative approaches to the one presented here aiming to increasing sample sizes in phosphoproteomic analyses of myocardial tissue by removing or minimizing experimental and sample processing and/or isobaric-labelling steps would result in a severe decrease of the reliably quantifiable (phospho)proteome. Therefore, the balance of quantity (sample numbers analysed) and quality (phosphoproteomic coverage depth and reliability) must be considered when interpreting the data, as always.

Most in vitro studies of cardiac fibrosis are dependent on the analysis of cells grown in a 2D cell-culture environment⁴⁷. However, the monolayer cell culture cannot adequately reproduce the actual disease process in a real human heart due to oversimplification of the extracellular microenvironment²⁶. Mechanisms governing ECM remodelling, myofibroblast activation and contractile functions can only be fully recapitulated with representative 3D scale models⁴⁸. With the aim of discovering mechanisms of cardiac fibrosis and develop potential therapeutic strategies, the Biowire II system was

designed as a model system for constructing a fibrosis-on-a-chip model which contains more sophisticated topographic and biomechanical cues than cells on flat dishes.

The majority of proteomic studies of fibrosis to date have utilized patient plasma or conventional cell culture, which are insufficient to obtain the comprehensive data of complex signalling leading to ECM remodelling in healthy and pathological tissues¹⁹. As demonstrated here, the combination of an OOC disease model with authentic ECM cues and refined phosphoproteomic and computational techniques have facilitated an in-depth systems-level profiling of the molecular networks in the cardiac fibrosis process, recapitulating similar events observed in patient explants and the TAC mouse model. This combined strategy has provided information that may lead to new insights into the early detection and prediction of fibrotic remodelling events.

By generating quantitative data on thousands of proteins and phosphorylation sites we were able to generate an in-depth profile of molecular pathways and factors underlying cardiac fibrosis utilizing both proteomic and phosphoproteomic analyses of patient explant, TAC mouse model and Biowire tissues. Using this strategy, we have provided a framework for future studies of cardiac fibrosis and a guide for future investigations on a variety of pathways (for example, pathways mediating electrotonic interactions between myofibroblasts and cardiomyocytes or regulation of fibrillar-protein deposition).

The cross-platform disease-modelling strategy will enable new insights into a wide variety of cardiac disease mechanisms, as well as provide a test bed for screening new therapies and potentially cut the cost and time of bringing new drugs to market. We were able to select compounds targeting a pathway identified through phosphoproteomic profiling. By evaluating the anti-fibrotic efficacy of a list of non-profiled GSK3 inhibitors from the GlaxoSmithKline published kinase inhibitor set²³ along with a standard commercially available inhibitor, we show the potential application of the fibrosis-on-a-chip model in preliminary compound screening. Anti-fibrotic effects of compounds can be studied at tissue level as well as molecular level with simplified functional assessment and sequential comprehensive phosphoproteomic analysis.

This study involves phosphoproteomic analyses of an OOC model system and of animal and human tissue, and provides an overview of dysregulated phosphorylation cascades in relation to myectomy samples from patients suffering from HCM and the most comprehensive phosphoproteomic analysis of the most commonly utilized mouse model of cardiac hypertrophy. More importantly, utilizing a combination of modern bioengineering, proteomic, and computational techniques, we have developed a multi-pronged approach for the reproducible characterization of potential therapeutics and their effects on central cardiac-signalling pathways that can be related back to human clinical samples and tissues from animal models of cardiovascular diseases. Thus, with appropriate modifications, this methodology is not limited to the study of cardiac fibrosis alone, but can potentially be applied to investigate a variety of other cardiac and other pathologies.

Methods

Biowire generation and preparation. Biowire tissues were generated starting from cardiomyocytes derived from the hiPSC line BJ1D and human ventricular fibroblasts¹³. Cardiomyocytes were mixed with cardiac fibroblasts in 3:1 (control) and 1:3 (fibrotic) cell-number ratios in a mixed hydrogel as previously described¹². After seeding, the engineered cardiac tissues were cultured for 7 d to allow for remodelling and compaction around the poly(octamethylene maleate (anhydride) citrate) (POMaC) wires. By day 7, the Biowires synchronously contracted and deflected the POMaC wire with each contraction. Biowires were washed five times in PBS and resuspended in 8 M urea containing a phosphatase (PhosStop, Roche) and Dounce homogenized to ensure the separation of fibrotic clots and contractile apparatus proteins from other intracellular proteins. The lysates were cleared of the cellular debris and protein aggregates by centrifugation at 13,000g for 10 min at 4°C (repeated three times). Centrifugation was repeated until no visible pellet was

present. The supernatant was frozen at -80°C for further processing. Passive force and active tension were determined from polymer-wire deflection as described^{12,13}. For phosphoproteomic mass spectrometry analysis, 5 individual Biowires were combined as a single replicate to obtain 100 μg protein.

SHG imaging and collagen quantification. Biowires and tissues were fixed with 4% paraformaldehyde and imaged by a SHG laser-scanning microscope (Zeiss LSM710 wo-Photon/Confocal microscope). A two-photon laser tuned to 860 nm was attached to the microscope and resulted in a SHG signal that was detectable at 475 nm. Quantification of collagen fibres was performed with ImageJ. A minimal threshold was set to segment the second-harmonic signal. The threshold was maintained for all images across all conditions. The ratio of thresholded collagen area to total tissue area was calculated and three images per sample were averaged together. Statistical analysis was performed using Prism 7.0.

Immunostaining. Biowire constructs were fixed with 4% paraformaldehyde, permeabilized with 0.25% Triton X-100 and blocked with 5% BSA. Immunostaining was performed using mouse anti-sarcomeric α -actinin (EA-53) (Abcam, catalogue (cat.) no. ab9465; 1:200), mouse anti-type I collagen (GeneTex, cat. no. GTX26308; 1:200), rabbit anti-smooth muscle actin (Abcam, cat. no. ab5694; 1:200) primary antibodies, together with donkey anti-mouse IgG heavy and light chain (Alexa Fluor 488) (Abcam, cat. no. ab150105; 1:400) and donkey anti-rabbit IgG heavy and light chain (Alexa Fluor 488) (Abcam, cat. no. ab150073; 1:400) secondary antibodies. Nuclei were counterstained with DAPI (Biotium; 1:100). For confocal microscopy, the stained cardiac Biowires were visualized under an inverted confocal microscope (Olympus IX81) or an upright confocal microscope (Zeiss LSM510).

Sham and four-week TAC mouse hearts were fresh frozen and sectioned using cryostat. After fixing with 10% formalin and permeabilization with 0.1% Triton X-100, primary antibody (α -actinin; ThermoScientific, 1:400) was incubated for 2 h at room temperature. Secondary antibody (Alexa Fluor 647, mouse; 1:100) was subsequently incubated for 1 h at room temperature. WGA was added dropwise and incubated for 1 h at room temperature. Slides were mounted using Cytoseal 60 and imaged using Zeiss spinning-disk confocal microscope.

Mouse heart tissue sample preparation. All animal experiments were conducted in accordance with the Animal Care Guidelines approved by the University of Toronto Animal Use and Care Committee. In brief, 6- to 8-week-old male CD1 (Charles River Laboratories) mice were randomly assigned to either sham or TAC experimental groups. All mice were then anaesthetized using 1.5% isoflurane and TAC was applied by placing a 7-0 silk suture around the transverse aorta. Successful TAC was confirmed by Doppler blood flow velocity via echocardiogram. Further echocardiographic assessment of cardiac function was performed (Supplementary Data 6) using B-mode and M-mode echocardiographic measurements (Vevo2100 imaging system, Visual Sonics). Four weeks following surgery, five TAC mice and five sham mice were killed using CO_2 and hearts were collected after surgery for phosphoproteomic analysis. Hearts were isolated and washed with ice-cold PBS. They were subsequently snap-frozen in liquid nitrogen and stored at -80°C . Each frozen heart was mechanically homogenized with a homogenizer (PRO 200; PRO Scientific) in 1 ml of 8 M urea solution with protease (Sigma) and phosphatase inhibitors (PhosSTOP; Roche). They were then centrifuged at 13,000g for 10 min and the supernatant was removed. The centrifugation step was repeated until no visible pellet was present to collect intracellular protein content and remove cellular debris, contractile apparatus proteins and any fibrotic clots that would interfere with mass spectrometry analysis due to an increased dynamic range of protein levels and resulting ion suppression. The supernatant was frozen at -80°C for further processing.

Patient tissue sample preparation. Patients that had undergone genetic testing for a panel of HCM genes were asked for consent for tissue collection at the time of septal myectomy under the institutional research ethics board approval (University Health Network, REB #13-6800). Tissue explants were collected immediately following resection, snap-frozen and stored in liquid nitrogen. Fifty milligrams of tissue was processed in the same manner as the mouse hearts described above. Anonymized clinical data were also collected. Tissue samples were grouped as 'gene positive' if specific pathogenic mutations were identified at the time of genetic testing, 'gene negative' if gene testing was negative, or LVOT controls as a result of unfolding of the aorta creating a specific septal geometry.

Protein digestion. Bradford total protein assay (Bio-Rad) was performed to determine the total protein content in each sample. One-hundred micrograms of protein from individual samples were used. A final concentration of 2.5 mM DTT was added to reduce two proteins from each sample for 60 min at room temperature. Iodoacetamide was then added to each sample to a final concentration of 5 mM for alkylation and incubated for 30 min at room temperature in the dark. Lastly, samples were diluted in 50 mM ammonium bicarbonate (to bring the urea concentration below 1 M) before the addition of 1:20 protein:protein ratio of sequencing-grade trypsin (Promega) for overnight digestion at 37°C . Formic acid was added to 1% in the sample solutions to block trypsin activity. Digested peptide fragments were isolated and desalted with C18

TopTips (Glygen). All samples were dried to completion by SpeedVac (Thermo). Cardiac tissue samples were resuspended in 80% acetonitrile (ACN) with 0.1% trifluoroacetic acid (TFA) and individual samples were subjected to HILIC–HPLC fractionation (that is, six separate HILIC–HPLC runs). Biowire and patient explant samples were subjected to TMT labelling.

TMT labelling. One-hundred micrograms of total protein (per TMT label), as determined by the Bradford total protein assay, from Biowire (five Biowires per TMT channel), patient explant and mouse tissue samples were labelled with TMT10-plex reagents as described by the manufacturer (Thermo). In brief, dried peptides in each sample were resuspended in 100 µl of triethylammonium bicarbonate (Sigma), individual TMT labels were resuspended in 41 µl of ACN and added to the corresponding samples, the labelling reaction was allowed to proceed for 1 h at room temperature, the reaction was stopped by quenching with 8 µl of 5% hydroxylamine (Sigma) and the individual samples were combined for each sample-type group (that is, Biowire constructs, patient explants and mouse cardiac tissue). The combined samples were dried to completion by SpeedVac and resuspended in 80% ACN with 0.1% TFA for HILIC fractionation.

Fractionation and phosphopeptide enrichment. HILIC fractionation for all sample types (1 mg of total protein per TMT dataset) was conducted using a 2.0 × 150 mm 5 µm particle TSKgel Amide-80 column (Tosoh Biocience) with an Agilent 1200 HPLC system. Two mobile phases were used: buffer A, composed of 98% ACN, 0.1% TFA and buffer B containing 2% ACN and 0.1% TFA. One milligram of digested peptides was loaded onto the column at a flow rate of 250 µl min⁻¹. The liquid chromatography was set up in the following manner: 3 min loading in 20% buffer B, a gradient of 20–40% buffer B for 27 min, a 3 min gradient of 40–100% buffer B, 100% buffer B for 5 min, 100–20% buffer B gradient for 2 min, and finally 10 min of 20% buffer B. Eluted samples were fractionated into 1.5 ml tubes at 2 min intervals and dried to completion. Ten percent of each fraction was used for global proteomic analysis. Phosphopeptide enrichment from resulting HILIC fractions was performed using TiO₂-coated Mag Sepharose beads (GE Life Sciences) according to the manufacturer's instructions. In brief, each HILIC fraction was dried to completion by SpeedVac (Thermo) and was resuspended in 200 µl of binding buffer (1 M glycolic acid, 80% ACN and 5% TFA), incubated with prepared magnetic beads for 1 h, washed one time with 500 µl binding buffer and three times with washing buffer (80% ACN and 1% TFA), and eluted three times in 100 µl of a 5% ammonium hydroxide solution. Eluted phosphopeptides were subsequently dried to completion and resuspended in 20 µl of 1% formic acid before liquid chromatography–mass spectrometry analysis.

TMT liquid chromatography–mass spectrometry. Resuspended phosphopeptide and peptide mixtures from each HILIC fraction were analysed in technical duplicates. The liquid chromatography component consisted of a reverse-phase Thermo Acclaim PepMap pre-column (2 cm length, 75 µm diameter, 3 µm C18 beads) and a Thermo PepMap RSLC C18 analytical column (50 cm length, 75 µm diameter, 2 µm C18 beads) connected to an Easy-nLC 1200 system (Thermo). The gradient (3 h), using a flow rate of 220 nl min⁻¹, was composed of buffer A (5% ACN, 0.1% formic acid) and buffer B (85% ACN, 0.1% formic acid). Equilibration was performed with 100% buffer A on both the pre- (20 µl) and analytical columns (3 µl) before each injection, followed by the nanoflow gradient as follows: 5–35% buffer B for 156 min, 35–100% buffer B for 9 min and 100% buffer B for 15 min. The EasySpray ion source (Thermo) was used to directly ionize peptides and phosphopeptides injected into a Q Exactive HF mass spectrometer (Thermo). For each selected full MS1 scan mass spectrum in profile mode 15 MS2 data-dependent scans were acquired with HCD fragmentation at 32% normalized collision energy. Full scan settings used were: 120,000 resolution, maximum injection time of 50 ms, ion packet setting of 3 × 10⁶ for automatic gain control, and a 350 to 1,450 m/z range. MS2 scan settings were: 60,000 resolution, ion packet setting of 1 × 10⁵ for automatic gain control, maximum injection time of 100 ms, fixed first mass at 100 m/z and 1.2 m/z isolation window. Unassigned, 1+ and parent ions with charge states higher than 6 were excluded from MS2 analysis, and the dynamic exclusion range was set to 20 s. Identical liquid chromatography and mass spectrometry settings and methods were used for proteomic (unenriched) and phosphoproteomic (phosphopeptide-enriched) samples or fractions.

RAW files from all MS analyses were searched using MaxQuant v.1.6.2.0 (www.coxdocs.org/doku.php?id=maxquant:start) against the mouse UniProt FASTA database (www.uniprot.org/taxonomy/10090) and human protein sequence database (<http://www.uniprot.org/taxonomy/9606>) with the use of 'Reporter ion MS2' 10plex TMT settings (0.003 reporter-ion tolerance) allowing for two missed trypsin-cleavage sites and variable modifications for protein phosphorylation at S, T and Y residues, N-terminal acetylation, asparagine and glutamine deamidation, and methionine oxidation. Carbamidomethylation was set as a fixed modification on cysteine residues. A false-discovery cutoff of 1% was used to filter for identified candidate peptides and phosphopeptides based on the searching of a reverse-sequence decoy database.

Data organization and analysis. MaxQuant search data were analysed by Perseus (v.1.6.0.7) and Bioconductor packages in R. Reporter ion (for TMT-labelled data)

intensities from protein groups (for proteomic analyses) and phosphorylation (Ser, Thr and Tyr) sites (from phosphoproteomic analyses) MaxQuant output files were log₂-transformed and quartile-normalized by 'width adjustment' in Perseus⁵⁰. Protein and phosphorylation-site identifications were filtered by removing entries corresponding to reverse database identifications, potential contaminants and those identified by site alone. Reported values for identical phosphorylation sites that were identified on singly or multiply phosphorylated phosphopeptides were entered as separate entries. Following independent normalization, phosphoproteomic and proteomic datasets for each sample type were merged at the gene and protein level to create merged datasets (with possible multiple entries due to multiple identified phosphorylation sites on the identified phosphoproteins), which were used in subsequent hierarchical clustering ($P < 0.05$, all reported heat maps) and principal component analyses (all data). Merged datasets were further trimmed by removing phosphorylation sites with less than 0.7 localization probability and duplicate entries at the gene level were removed (that is, most significantly altered protein and phosphorylation sites remained). Thus processed merged datasets were subjected to independent biological pathway enrichment by GSEA⁵¹ using a custom database (http://download.baderlab.org/EM_gene_sets/)⁵¹ carrying annotated GO biological process terms and curated pathways. Enriched gene sets were required to have between 10 and 500 associated components, $P < 0.05$ and false-discovery rate < 0.1 . To accommodate direct comparisons, identified mouse proteins were mapped to human orthologues on the basis of gene name from the ENSEMBL database. The data are available via ProteomeXchange with identifier PXD016492. All hierarchical clustering was performed in Perseus (v.1.6.0.7) using average Euclidian distance with no constraints on row clustering (and column clustering where cluster trees are visualized) with data pre-processed with k -means, 10 iterations and a maximal number of 300 clusters.

Kinase target motif analysis. Significantly altered phosphorylation sites (two-tailed Student's t -test, $P < 0.05$) from different experiments were annotated using the linear motifs function from the sequence window centred around the modified phosphorylation sites identifying their corresponding kinase in Perseus⁵⁰.

Drug testing. Kinase inhibitors were kindly provided by GlaxoSmithKline⁵². Four different published GSK3-inhibitor compounds (GW806290X, GW827102X, GW828529X and GW827099X) were blindly selected from 63 compounds in the kit. Ten millimolar stock solution was made in sterile DMSO. The compounds were further diluted in maintenance medium to achieve a final inhibitor concentration of 1 µM, based on a previous report⁵². Standard GSK3 inhibitor CHIR 99021 was purchased from Cayman Chemical (cat. no. 131222). Ten millimolar stock solution was made in sterile DMSO. The compounds were further diluted in maintenance medium to achieve a final inhibitor concentration of 5 µM.

Reporting Summary. Further information on research design is available in the Nature Research Reporting Summary linked to this article.

Data availability

The main data supporting the results in this study are available within the paper and its Supplementary Information. All data generated during the study, including source data and the data used to make the figures, are available via ProteomeXchange with identifier PXD016492.

Received: 19 December 2018; Accepted: 14 June 2020;

References

- Mozaffarian, D. et al. Heart disease and stroke statistics—2015 update: a report from the American Heart Association. *Circulation* **131**, e29–e322 (2015).
- Niimura, H. et al. Sarcomere protein gene mutations in hypertrophic cardiomyopathy of the elderly. *Circulation* **105**, 446–451 (2002).
- Braunwald, E. Cardiomyopathies: an overview. *Circ. Res.* **121**, 711–721 (2017).
- Ho, C. Y. et al. Myocardial fibrosis as an early manifestation of hypertrophic cardiomyopathy. *N. Engl. J. Med.* **363**, 552–563 (2010).
- van Berlo, J. H., Maillet, M. & Molkenkin, J. D. Signaling effectors underlying pathologic growth and remodeling of the heart. *J. Clin. Invest.* **123**, 37–45 (2013).
- Travers, J. G., Kamal, F. A., Robbins, J., Yutzey, K. E. & Blaxall, B. C. Cardiac fibrosis: the fibroblast awakens. *Circ. Res.* **118**, 1021–1040 (2016).
- Shirani, J., Pick, R., Roberts, W. C. & Maron, B. J. Morphology and significance of the left ventricular collagen network in young patients with hypertrophic cardiomyopathy and sudden cardiac death. *J. Am. Coll. Cardiol.* **35**, 36–44 (2000).
- Kim, J. B. et al. Polony multiplex analysis of gene expression (PMAGE) in mouse hypertrophic cardiomyopathy. *Science* **316**, 1481–1484 (2007).
- Ahadian, S. et al. Organ-on-a-chip platforms: a convergence of advanced materials, cells, and microscale technologies. *Adv. Healthc. Mater.* **1700506** (2018).

10. Sun, X. & Nunes, S. S. Biowire platform for maturation of human pluripotent stem cell-derived cardiomyocytes. *Sci. Rep.* **101**, 21–26 (2016).
11. Nunes, S. S. et al. Biowire: a platform for maturation of human pluripotent stem cell-derived cardiomyocytes. *Nat. Methods* **10**, 781–787 (2013).
12. Zhao, Y. et al. A platform for generation of chamber-specific cardiac tissues and disease modeling. *Cell* **176**, 913–927 (2019).
13. Conant, G., Ahadian, S., Zhao, Y. & Radisic, M. Kinase inhibitor screening using artificial neural networks and engineered cardiac biowires. *Sci. Rep.* **7**, 11807 (2017).
14. Wang, E. Y. et al. Biowire model of interstitial and focal cardiac fibrosis. *ACS Cent. Sci.* **5**, 1146–1158 (2019).
15. Kuzmanov, U. et al. Global phosphoproteomic profiling reveals perturbed signaling in a mouse model of dilated cardiomyopathy. *Proc. Natl Acad. Sci. USA* **113**, 12592–12597 (2016).
16. Chang, Y. W. et al. Quantitative phosphoproteomic study of pressure-overloaded mouse heart reveals dynamin-related protein 1 as a modulator of cardiac hypertrophy. *Mol. Cell. Proteom.* **12**, 3094–3107 (2013).
17. Lundby, A. et al. In vivo phosphoproteomics analysis reveals the cardiac targets of β -adrenergic receptor signaling. *Sci. Signal.* **6**, rs11 (2013).
18. Gedik, N. et al. Proteomics/phosphoproteomics of left ventricular biopsies from patients with surgical coronary revascularization and pigs with coronary occlusion/reperfusion: remote ischemic preconditioning. *Sci. Rep.* **7**, 7629 (2017).
19. Mercier, T. et al. Interplay between phosphorylation and O-GlcNAcylation of sarcomeric proteins in ischemic heart failure. *Front. Endocrinol.* **9**, 598 (2018).
20. Schechter, M. A. et al. Phosphoproteomic profiling of human myocardial tissues distinguishes ischemic from non-ischemic end stage heart failure. *PLoS ONE* **9**, e104157 (2014).
21. Cai, W. et al. An unbiased proteomics method to assess the maturation of human pluripotent stem cell-derived cardiomyocytes. *Circ. Res.* **125**, 936–953 (2019).
22. Cyganek, L. et al. Deep phenotyping of human induced pluripotent stem cell-derived atrial and ventricular cardiomyocytes. *JCI insight* **3**, e99941 (2018).
23. Elkins, J. M. et al. Comprehensive characterization of the published kinase inhibitor set. *Nat. Biotechnol.* **34**, 95–103 (2016).
24. Engholm-Keller, K. & Larsen, M. R. Technologies and challenges in large-scale phosphoproteomics. *Proteomics* **13**, 910–931 (2013).
25. Xiao, Y. et al. Microfabricated perfusable cardiac biowire: a platform that mimics native cardiac bundle. *Lab Chip* **14**, 869–882 (2014).
26. Conant, G. et al. High-content assessment of cardiac function using heart-on-a-chip devices as drug screening model. *Stem Cell Rev.* **13**, 335–346 (2017).
27. Mi, H. et al. PANTHER version 11: expanded annotation data from Gene Ontology and reactome pathways, and data analysis tool enhancements. *Nucleic Acids Res.* **45**, D183–d189 (2017).
28. Fabregat, A. et al. The reactome pathway knowledgebase. *Nucleic Acids Res.* **46**, D649–d655 (2018).
29. The Gene Ontology Consortium. Expansion of the gene ontology knowledgebase and resources. *Nucleic Acids Res.* **45**, D331–d338 (2017).
30. Ashburner, M. et al. Gene ontology: tool for the unification of biology. *Nat. Genet.* **25**, 25–29 (2000).
31. Subramanian, A. et al. Gene set enrichment analysis: a knowledge-based approach for interpreting genome-wide expression profiles. *Proc. Natl Acad. Sci.* **102**, 15545–15550 (2005).
32. Naba, A. et al. The matrisome: in silico definition and in vivo characterization by proteomics of normal and tumor extracellular matrices. *Mol. Cell. Proteom.* **11**, M111.014647 (2012).
33. Tanigaki, K. et al. Fc γ receptors and ligands and cardiovascular disease. *Circ. Res.* **116**, 368–384 (2015).
34. Li, P., Ge, J. & Li, H. Lysine acetyltransferases and lysine deacetylases as targets for cardiovascular disease. *Nat. Rev. Cardiol.* **17**, 96–115 (2020).
35. Chen, C., Li, R., Ross, R. S. & Manso, A. M. Integrins and integrin-related proteins in cardiac fibrosis. *J. Mol. Cell Cardiol.* **93**, 162–174 (2016).
36. Franchini, K. G. Focal adhesion kinase—the basis of local hypertrophic signaling domains. *J. Mol. Cell Cardiol.* **52**, 485–492 (2012).
37. Döring, Y., Pawig, L., Weber, C. & Noels, H. The CXCL12/CXCR4 chemokine ligand/receptor axis in cardiovascular disease. *Front. Physiol.* **5**, 212 (2014).
38. He, W. & Dai, C. Key fibrogenic signaling. *Curr. Pathobiol. Rep.* **3**, 183–192 (2015).
39. Juhaszova, M. et al. Role of glycogen synthase kinase-3 β in cardioprotection. *Circ. Res.* **104**, 1240–1252 (2009).
40. Takeishi, Y. et al. Src and multiple MAP kinase activation in cardiac hypertrophy and congestive heart failure under chronic pressure-overload: comparison with acute mechanical stretch. *J. Mol. Cell Cardiol.* **33**, 1637–1648 (2001).
41. Wang, Y. Mitogen-activated protein kinases in heart development and diseases. *Circulation* **116**, 1413–1423 (2007).
42. Gan, B. et al. Role of FIP200 in cardiac and liver development and its regulation of TNF α and TSC–mTOR signaling pathways. *J. Cell Biol.* **175**, 121–133 (2006).
43. Kuwahara, K. Role of NRSF/REST in the regulation of cardiac gene expression and function. *Circulation J.* **77**, 2682–2686 (2013).
44. Li, Y. et al. Targeted disruption of TCF12 reveals HEB as essential in human mesodermal specification and hematopoiesis. *Stem Cell Rep.* **9**, 779–795 (2017).
45. Schunke, K. J. et al. Protein kinase C binding protein 1 inhibits hypoxia-inducible factor-1 in the heart. *Cardiovasc Res.* **115**, 1332–1342 (2019).
46. Lam, M. P. et al. An MRM-based workflow for quantifying cardiac mitochondrial protein phosphorylation in murine and human tissue. *J. Proteom.* **75**, 4602–4609 (2012).
47. Mosadegh, B. et al. Three-dimensional paper-based model for cardiac ischemia. *Adv. Healthc. Mater.* **3**, 1036–1043 (2014).
48. Caulfield, J. B. & Borg, T. K. The collagen network of the heart. *Lab. Invest.* **40**, 364–372 (1979).
49. Gucek, M. Proteomics approaches to fibrotic disorders. *Fibrogenesis Tissue Repair* **5**, S10 (2012).
50. Tyanova, S., Temu, T. & Sinitcyn, P. The Perseus computational platform for comprehensive analysis of (prote)omics data. *Nat. Methods* **13**, 731–740 (2016).
51. Isserlin, R., Merico, D., Voisin, V. & Bader, G. D. Enrichment Map—a Cytoscape app to visualize and explore OMICs pathway enrichment results. *F1000Research*. **3**, 141 (2014).
52. Tavares, F. X. et al. *N*-Phenyl-4-pyrazolo[1,5-*b*]pyridazin-3-ylpyrimidin-2-amines as potent and selective inhibitors of glycogen synthase kinase 3 with good cellular efficacy. *J. Med. Chem.* **47**, 4716–4730 (2004).

Acknowledgements

We thank H. Rakowski for initial discussions on study design and execution; GlaxoSmithKline and W. Zuercher for the gift of the published kinase inhibitor set; and J. Greenblatt and E. Macron for allowing access to instrumentation at the Donnelly Centre. This research is part of the University of Toronto's Medicine by Design initiative which receives funding from the Canada First Research Excellence Fund. This project was funded by the Ted Rogers Centre for Heart Research Translational Biology and Engineering Program to A.G., the Heart and Stroke Richard Lewar Centres of Excellence in Cardiovascular Research and CHRR Grants to A.G. (PJT-155921 and PJT-166118; MOP-106538; MOP-123320). S.-H.L. was supported by a NSERC Postgraduate Scholarship, an Ontario Graduate Scholarship and a Ted Rogers Centre for Heart Research Doctoral Fellowship. S.H.-L. was supported by a Canada Graduate Scholarship–Master's Award from Canadian Institutes of Health Research and an Ontario Graduate Scholarship. U.K. was supported by a Ted Rogers Centre for Heart Research Postdoctoral Fellowship. This work was funded by the Canadian Institutes of Health Research Foundation Grant (FDN-167274), Natural Sciences and Engineering Research Council–Canadian Institutes of Health Research Collaborative Health Research Grant (CHRP 493737-16) and Killam Fellowship (7025-19-0016) awarded to M.R. E.Y.W. was supported by Alexander Graham Bell Canada Graduate Scholarship–Doctoral Award (CGS–D). A.E. acknowledges a Foundation Grant (FDN-148399) from the Canadian Institutes of Health Research.

Author contributions

A.E., A.G., E.Y.W., M.R. and U.K. designed the study and wrote the manuscript. U.K. performed experimental preparation and bioinformatic data analysis of all (phospho) proteomics samples. E.Y.W. generated the Biowire constructs and performed all associated experimental work, including fluorescence imaging of Biowire, mouse, and patient explant samples. R.V. and F.B. assisted in the design of the study and provided patient surgical explant samples and associated clinical information. D.H.K., S.H.-L., S.-H.L. and P.S. helped in the design and performing of mouse experiments and preparation of mass spectrometry samples. H.G. and M.M. maintained and operated mass spectrometry instrumentation. Y.Z. assisted in the generation of Biowire constructs and design of the study. UK wrote the initial manuscript, which was edited by all authors.

Competing interests

M.R. and Y.Z. are co-founders and hold shares in TARA Biosystems, which uses the Biowire II platform for commercial drug testing.

Additional information

Supplementary information is available for this paper at <https://doi.org/10.1038/s41551-020-0585-y>.

Correspondence and requests for materials should be addressed to M.R., A.G. or A.E.

Reprints and permissions information is available at www.nature.com/reprints.

Publisher's note Springer Nature remains neutral with regard to jurisdictional claims in published maps and institutional affiliations.

© The Author(s), under exclusive licence to Springer Nature Limited 2020

QUERY FORM

Nature Biomedical Engineering	
Manuscript ID	[Art. Id: 585]
Author	Uros Kuzmanov

AUTHOR:

The following queries have arisen during the editing of your manuscript. Please answer by making the requisite corrections directly in the e-proofing tool rather than marking them up on the PDF. This will ensure that your corrections are incorporated accurately and that your paper is published as quickly as possible.

Query No.	Nature of Query
Q1:	There was no affiliation for Hongbo Guo. Please ensure the correct affiliation is added for this author.
Q2:	Reference [46] is a duplicate of [16] and hence the repeated version has been deleted. Please check.
Q3:	Please note that all affiliations must be listed individually. If affiliation 9 is more than one department or organization, please split it into individual affiliations.
Q4:	Please check your article carefully, coordinate with any co-authors and enter all final edits clearly in the eproof, remembering to save frequently. Once corrections are submitted, we cannot routinely make further changes to the article.
Q5:	Note that the eproof should be amended in only one browser window at any one time; otherwise changes will be overwritten.
Q6:	Author surnames have been highlighted. Please check these carefully and adjust if the first name or surname is marked up incorrectly. Note that changes here will affect indexing of your article in public repositories such as PubMed. Also, carefully check the spelling and numbering of all author names and affiliations, and the corresponding email address(es).
Q7:	You cannot alter accepted Supplementary Information files except for critical changes to scientific content. If you do resupply any files, please also provide a brief (but complete) list of changes. If these are not considered scientific changes, any altered Supplementary files will not be used, only the originally accepted version will be published.
Q8:	Please define nLC-ESI-MS-HCD-MS and MS2 in the caption of Fig. 1
Q9:	We reserve 'significant' and its derivatives to mean statistically significant; for all instances in this paper, please re-word (e.g. 'important', 'notable', 'substantial', 'marked') or supply a statistical measure such as P value. See the sentence beginning 'The gel compaction...' for the first use
Q10:	Please confirm that the edits to the sentence 'From the parallel proteomic analysis...' preserve the originally intended meaning.
Q11:	The caption for Fig. 3c has been reworded for clarity, specifically, the part about the mutation and 'gene-negative'. Please check.
Q12:	In caption for Fig. 3c (right heat map), please indicate what the (2) means, e.g. in S424(2).
Q13:	In the sentence 'Additionally, a large overlap...' are the iPSCs referred to hiPSCs? 'iPSCs' has not been defined,

QUERY FORM

Nature Biomedical Engineering	
Manuscript ID	[Art. Id: 585]
Author	Uros Kuzmanov

AUTHOR:

The following queries have arisen during the editing of your manuscript. Please answer by making the requisite corrections directly in the e-proofing tool rather than marking them up on the PDF. This will ensure that your corrections are incorporated accurately and that your paper is published as quickly as possible.

Query No.	Nature of Query
	thus this has been expanded.
Q14:	Please define NES in caption of Fig. 5b.
Q15:	HDAC was expanded to histone deacetylase. OK?
Q16:	Please define CM and cFB in caption of Fig. 6a.
Q17:	myoFB was expanded to myofibroblast. OK?
Q18:	In the sentence 'The GW806290X-treated group...' can 'most significant' be replaced with 'greatest', or is this significance supported by P values?
Q19:	Please confirm that the edits to the sentence 'Biowire tissues were generated....' preserve the originally intended meaning.
Q20:	Please check the sentence 'A final concentration of 2.5 mM....' for clarity.
Q21:	The initials AOG listed in acknowledgements have been corrected to A.G. in line with the author list. OK?
Q22:	Please confirm the correct article numbers have been added for refs. 9 and 37.
Q23:	Please confirm correct journal, volume and page details have been added for ref. 34.

Reporting Summary

Nature Research wishes to improve the reproducibility of the work that we publish. This form provides structure for consistency and transparency in reporting. For further information on Nature Research policies, see our [Editorial Policies](#) and the [Editorial Policy Checklist](#).

Statistics

For all statistical analyses, confirm that the following items are present in the figure legend, table legend, main text, or Methods section.

n/a Confirmed

- ☐ ☒ The exact sample size (n) for each experimental group/condition, given as a discrete number and unit of measurement
- ☐ ☒ A statement on whether measurements were taken from distinct samples or whether the same sample was measured repeatedly
- ☐ ☒ The statistical test(s) used AND whether they are one- or two-sided
Only common tests should be described solely by name; describe more complex techniques in the Methods section.
- ☐ ☒ A description of all covariates tested
- ☐ ☒ A description of any assumptions or corrections, such as tests of normality and adjustment for multiple comparisons
- ☐ ☒ A full description of the statistical parameters including central tendency (e.g. means) or other basic estimates (e.g. regression coefficient) AND variation (e.g. standard deviation) or associated estimates of uncertainty (e.g. confidence intervals)
- ☐ ☒ For null hypothesis testing, the test statistic (e.g. F , t , r) with confidence intervals, effect sizes, degrees of freedom and P value noted
Give P values as exact values whenever suitable.
- ☐ ☒ For Bayesian analysis, information on the choice of priors and Markov chain Monte Carlo settings
- ☐ ☒ For hierarchical and complex designs, identification of the appropriate level for tests and full reporting of outcomes
- ☐ ☒ Estimates of effect sizes (e.g. Cohen's d , Pearson's r), indicating how they were calculated

Our web collection on [statistics for biologists](#) contains articles on many of the points above.

Software and code

Policy information about [availability of computer code](#)

Data collection MaxQuant version 1.6.2.0, Perseus version 1.6.0.7

Data analysis Graphpad Prism 7.0

For manuscripts utilizing custom algorithms or software that are central to the research but not yet described in published literature, software must be made available to editors and reviewers. We strongly encourage code deposition in a community repository (e.g. GitHub). See the Nature Research [guidelines for submitting code & software](#) for further information.

Data

Policy information about [availability of data](#)

All manuscripts must include a [data availability statement](#). This statement should provide the following information, where applicable:

- Accession codes, unique identifiers, or web links for publicly available datasets
- A list of figures that have associated raw data
- A description of any restrictions on data availability

The main data supporting the results in this study are available within the paper and its Supplementary Information. All data generated during the study, including source data and the data used to make the figures, are available via ProteomeXchange with identifier PXD016492.

Field-specific reporting

Please select the one below that is the best fit for your research. If you are not sure, read the appropriate sections before making your selection.

☒ Life sciences ☐ Behavioural & social sciences ☐ Ecological, evolutionary & environmental sciences

For a reference copy of the document with all sections, see [nature.com/documents/nr-reporting-summary-flat.pdf](https://www.nature.com/documents/nr-reporting-summary-flat.pdf)

Life sciences study design

All studies must disclose on these points even when the disclosure is negative.

Sample size	Sample sizes were not predetermined, and were chosen according to standards in the field.
Data exclusions	No data were excluded.
Replication	All TMT-labeled datasets were run in technical duplicates on the mass spectrometer.
Randomization	Randomization was not applicable. We had clearly defined experimental groups based on clinical data, mouse treatment, or tissue-generation conditions.
Blinding	No blinding was performed, as the study was exploratory.

Reporting for specific materials, systems and methods

We require information from authors about some types of materials, experimental systems and methods used in many studies. Here, indicate whether each material, system or method listed is relevant to your study. If you are not sure if a list item applies to your research, read the appropriate section before selecting a response.

Materials & experimental systems

n/a	Involved in the study
<input type="checkbox"/>	<input checked="" type="checkbox"/> Antibodies
<input type="checkbox"/>	<input checked="" type="checkbox"/> Eukaryotic cell lines
<input checked="" type="checkbox"/>	<input type="checkbox"/> Palaeontology and archaeology
<input type="checkbox"/>	<input checked="" type="checkbox"/> Animals and other organisms
<input type="checkbox"/>	<input checked="" type="checkbox"/> Human research participants
<input checked="" type="checkbox"/>	<input type="checkbox"/> Clinical data
<input checked="" type="checkbox"/>	<input type="checkbox"/> Dual use research of concern

Methods

n/a	Involved in the study
<input checked="" type="checkbox"/>	<input type="checkbox"/> ChIP-seq
<input checked="" type="checkbox"/>	<input type="checkbox"/> Flow cytometry
<input checked="" type="checkbox"/>	<input type="checkbox"/> MRI-based neuroimaging

Antibodies

Antibodies used	Primary antibodies: Mouse Anti-Sarcomeric Alpha Actinin antibody [EA-53] (Abcam, cat no.ab9465); Mouse Anti-type I Collagen (GeneTex, cat.no GTX26308); Rabbit Anti-smooth muscle Actin antibody (Abcam, cat no. ab5694). Secondary antibodies: Donkey Anti-Mouse IgG H&L (Alexa Fluor® 488) (Abcam, cat no. ab150105), and Donkey Anti-Rabbit IgG H&L (Alexa Fluor 488) (Abcam, cat no. ab150073).
Validation	https://www.abcam.com/Sarcomeric-Alpha-Actinin-antibody-EA-53-ab9465.html http://www.genetex.com/Collagen-I-antibody-COL-1-GTX26308.html https://www.abcam.com/alpha-smooth-muscle-actin-antibody-ab5694.html https://www.abcam.com/donkey-mouse-igg-hl-alex-fluor-488-ab150105.html https://www.abcam.com/donkey-rabbit-igg-hl-alex-fluor-488-ab150073.html

Eukaryotic cell lines

Policy information about [cell lines](#)

Cell line source(s)	Ventricular cardiomyocytes were derived from the human induced pluripotent stem cell line BJ1D, by using monolayer-differentiation protocols (Lian et al., PNAS (2012); Lian et al., Nat. Prot. (2013)). Human Ventricular cardiac fibroblasts were obtained from LONZA (Clonetics NHCF-V).
Authentication	We have performed STR profiling for the BJ1D cell line, and BJ1D-CM for cell-line authentication. The cell-line-authentication data for the commercially available human ventricular cardiac fibroblasts are available from Lonza.

Mycoplasma contamination

The cell lines were not tested for mycoplasma contamination.

Commonly misidentified lines
(See [ICLAC](#) register)

No commonly misidentified cell lines were used.

Animals and other organisms

Policy information about [studies involving animals](#); [ARRIVE guidelines](#) recommended for reporting animal research

Laboratory animals

6–8 week old male CD1 mice from Charles River Laboratories.

Wild animals

The study did not involve wild animals.

Field-collected samples

The study did not involve samples collected from the field.

Ethics oversight

All animal experiments were conducted in accordance with the Animal Care Guidelines approved by the University of Toronto Animal Use and Care Committee.

Note that full information on the approval of the study protocol must also be provided in the manuscript.

Human research participants

Policy information about [studies involving human research participants](#)

Population characteristics

Provided in Supplementary Table 1.

Recruitment

Septal myectomy samples were collected with permission from the study participants.

Ethics oversight

University Health Network, Toronto, Canada (REB #13-6800).

Note that full information on the approval of the study protocol must also be provided in the manuscript.